Hybrid Density Functional Theory for Homopolymer Mixtures Confined in a Selective Nanoslit

Houyang Chen, Zhencheng Ye, Jun Cai, Honglai Liu,* and Ying Hu

State Key Laboratory of Chemical Engineering and Department of Chemistry, East China University of Science and Technology, Shanghai 200237, China

Jianwen Jiang*

Department of Chemical and Biomolecular Engineering, National University of Singapore, 4 Engineering Drive 4, Singapore 117576

Received: December 20, 2006; In Final Form: March 29, 2007

By integrating polymer density function theory (DFT) and single-chain molecular simulation, a hybrid DFT is developed for homopolymer mixtures confined in a selective nanoslit. Two weighting functions are adopted separately in the polymer DFT for repulsive and attractive contributions to the excess free energy functional. The theoretical results agree well with simulation data for the density profiles, configurations (tail, loop and train), adsorption amounts, layer thicknesses, and partition coefficients. The polymer−slit interaction is found to have a large effect on the density profiles and partition coefficients but is found to have a small effect on the average sizes and percentages of the configurations. Nearly half of the polymer segments form tails, and the other half form trains. In addition, bridges are observed to form for sufficiently long polymer chains. As the length difference between two polymers increases, the effect of chain connectivity becomes increasingly important.

1. Introduction

Selective adsorption and separation of polymer mixtures on a substrate have numerous important applications in manufacturing processes.[1−5] For instance, vegetable tannins that are harmful to animals and humans can be removed by selective adsorption onto collagen fibers.[6,7] Adsorption of serum albumin on modified biomedical polyurethane surfaces can inhibit in situ blood coagulation, microbial infection, and subsequent inflammatory reaction.[8]

In the past, a number of statistical-mechanics-based theories have been proposed to study the effect of substrate heterogeneity on selective adsorption, such as ideal-adsorbed-solution theory or modified ideal-adsorbed-solution theory,[9−12] mean-field theory,[13] Doong-Yang model,[14] integral equation theory,[15−17] and equilibrium theory.[18,19] Alternatively, density functional theory (DFT) has been widely used to investigate the structural and thermodynamic properties of confined fluids. As an extension of the reference-interaction-site model (RISM)[20] for simple atomic fluids, DFT for molecular fluids was developed by Chandler, McCoy, and Singer (CMS).[21−24] The weighted-density approach (WDA) for molecular systems was first built by Woodward[25] and later by Kierlik and Rosinburg (KR).[26] In the WDA, all of the intra- and intermolecular correlations are included in the excess free energy functional with a coarse-graining approximation and a simple weighting function. For polymer mixtures, Nath et al.[27] proposed a DFT from the PRISM-based framework of CMS. By introducing a partial excess free energy functional, Cai et al.[28,29] extended the equation of state-based DFT to hard-sphere chain mixtures; subsequently Ye et al.[30−32] developed the equation of state-based DFT for square-well chain fluids. Yu and Wu[33] developed a new DFT by combining Rosenfeld's FMT[34] for the excluded-volume effect with Wertheim's TPT1[35] for the chain connectivity. Tripathi and Chapman[36] combined statistical-association-fluid theory (SAFT)[37] with FMT[34] and developed another new DFT for polymer mixtures. Apart from these, mean-field theory[38,39] and perturbation approach[40,41] have been used to incorporate the dispersion interaction into the Helmholtz energy functional for inhomogeneous polymers.

In this work, we develop a hybrid DFT that integrates the partial excess free energy functional[28,29] with single-chain molecular simulation. Intramolecular correlation is an important component in DFT and can be taken into account by single-chain simulation[42−47] or Dirac delta function method.[26,30,33,48] Between these two, the single-chain simulation is expected theoretically to be more accurate. Comparison between the work of Yethiraj et al.[46] and that of Yu and Wu,[48] however, reveals the Dirac delta function method may be better in some cases and an appropriately selected weighting function is crucial in DFT. Here, two weighted density approximations are adopted in the excess free energy functional, one was developed by Yethiraj[42] and the other was expanded by Ye et al.[30] While most DFTs fail for a system with a very strong interaction between the polymer and the slit, predictions of our hybrid DFT coincide well with simulations. Moreover, through a single-chain simulation, adsorption configurations including tail, loop, and train can be calculated from our hybrid DFT. To our knowledge, this is the first time the information of configurations becomes available from DFT.

The rest of the article is organized as follows. The theoretical framework of our hybrid DFT is developed in section 2. In

* Corresponding authors. E-mail: hlliu@ecust.edu.cn (H.L.) and chejj@nus.edu.sg (J.J.).

10.1021/jp068784b CCC: $37.00
Published on Web 05/08/2007

section 3, we examine a variety of homopolymer mixtures confined in selective and nonselective slits. Predictions of density profiles, configurations, partition coefficients, adsorption amounts, and layer thicknesses are presented and compared with simulation results. Finally, conclusions are given in section 4.

2. Model and Theory

Without the loss of generality, a homopolymer mixture with K components is considered in the present work. Each component is a square-well chain composed of m_i identical segmentswith identical diameter σ. The interaction between nonbonded segments is square-well potential

$$u(r_{ij}) = \begin{cases} 0 & r_{ij} > L\sigma \\ -\epsilon_{ij} & \sigma < r_{ij} < L\sigma \\ \infty & r_{ij} < \sigma \end{cases} \tag{1}$$

where r_{ij} is the distance between two segments. Under confinement within a nanoslit, the interaction of chain segment with each slit wall $u_{i-\mathrm{wall}}$ is given by

$$u(r_{i-\mathrm{wall}}) = \begin{cases} 0 & r_{i-\mathrm{wall}} > \sigma \\ -\lambda_{iw} & 0 < r_{i-\mathrm{wall}} < \sigma \\ \infty & r_{i-\mathrm{wall}} < 0 \end{cases} \tag{2}$$

where $r_{i-\mathrm{wall}}$ is the distance between the center of segment and slit wall.

The Helmholtz free energy functional $F[\rho_M(R)]$ of the system can be decomposed into an ideal part and an excess part,

$$F[\rho_M(R)] = kT\sum_{l=1}^{K}\int\{\rho_{M,l}(R_l) - [\ln \rho_{M,l}(R_l) - 1 + \beta U_{M,l}(R_l) + \beta V_{M,l}(R_l)]\}\,\mathrm{d}R_l + F^{ex}[\rho_M(R)] \tag{3}$$

where $\rho_M(R)$ is chain density as a function of positions R. R_l, $\rho_{M,l}$, $V_{M,l}$, and $U_{M,l}$ are position, density profile, external-field potential, and intramolecular interaction of component l, respectively.

The excess Helmholtz free energy functional is[30,42,49]

$$F^{ex} = F^{ex}_{hs} + F^{ex}_{attr} \tag{4}$$

where the subscript "hs" represents the hard-sphere repulsive contribution, and the subscript "attr" denotes the contribution of square-well attractive interaction between segments. The following weighted density approximations are adopted separately for these two contributions,

$$F^{ex}_{hs}[\rho_M] = \sum_{i=1}^{K}\int \rho_i(\boldsymbol{r}) f^{(i)}_{hs}[\bar{\rho}^{(i)}_{hs}(\boldsymbol{r})]\,\mathrm{d}\boldsymbol{r} \tag{5a}$$

$$F^{ex}_{attr}[\rho_M] = \sum_{i=1}^{K}\int \rho_i(\boldsymbol{r}) f^{(i)}_{attr}[\bar{\rho}^{(i)}_{attr}(\boldsymbol{r})]\,\mathrm{d}\boldsymbol{r} \tag{5b}$$

where $f^{(i)}_{hs}[\bar{\rho}]$ is the partial excess free energy functional of a hard-sphere chain i at a given weighted density profile $\bar{\rho}^{(i)}_{hs}(\boldsymbol{r})$, which accounts for the excluded-volume effect. $f^{(i)}_{attr}(\bar{\rho})$ is the difference between the partial excess free energy of a square-well chain and that of a hard-sphere chain. Expressions of $f^{(i)}_{hs}$ and $f^{(i)}_{attr}$ can be found elsewhere.[30] F^{ex}_{hs} is calculated by the Helmholtz free energy model of hard-sphere chain fluids developed by Hu et al.,[50] and F^{ex}_{attr} is calculated by the SAFT-VR equation of state developed by Gil-Villegas et al.[51] $\bar{\rho}(\boldsymbol{r})$ is the weighted density profile given by

$$\bar{\rho}_{hs}(\boldsymbol{r}) = \int \rho(\boldsymbol{r}') w_{hs}(|\boldsymbol{r} - \boldsymbol{r}'|)\,\mathrm{d}\boldsymbol{r}' \tag{6a}$$

$$\bar{\rho}_{attr}(\boldsymbol{r}) = \int \rho(\boldsymbol{r}') w_{attr}(|\boldsymbol{r} - \boldsymbol{r}'|)\,\mathrm{d}\boldsymbol{r}' \tag{6b}$$

where $w_{hs}(\boldsymbol{r})$ and $w_{attr}(\boldsymbol{r})$ are the weighting functions for hard sphere and attractive square-well contributions, respectively. The weighting functions satisfy the normalization condition,

$$\int w_{hs}(\boldsymbol{r})\,\mathrm{d}\boldsymbol{r} = \int w_{attr}(\boldsymbol{r})\,\mathrm{d}\boldsymbol{r} = 1 \tag{7}$$

with

$$w_{hs}(\boldsymbol{r}) = 3\Theta(\sigma - \boldsymbol{r})/4\pi\sigma^3 \tag{8a}$$

$$w_{attr}(\boldsymbol{r}) = 3\Theta(L\sigma - \boldsymbol{r})/4\pi(L\sigma)^3 \tag{8b}$$

where $L\sigma$ is the width of square-well and $L = 1.5$ is selected throughout this work.

Following our previous work,[31] the chemical potential of molecule $\mu_{M,l}$ can be expressed as the derivative of the free energy functional,

$$\mu_{M,l} = kT\ln\rho_{M,l}(\boldsymbol{R}_l) + U_{M,l}(\boldsymbol{R}_l) + V_{M,l}(\boldsymbol{R}_l) + \frac{\delta F^{ex}[\rho_M]}{\delta\rho_{M,l}(\boldsymbol{R}_l)} \tag{9}$$

The segment density is given by

$$\rho_l(\boldsymbol{r}) = \int\sum_{j=1}^{m_l}\rho_{M,l}(\boldsymbol{R}_l)\delta(\boldsymbol{r} - \boldsymbol{r}_j)\,\mathrm{d}\boldsymbol{R}_l \tag{10}$$

where ρ_l is the segment density profile of molecule l with length m_l, and $\boldsymbol{r}$ is the segment coordinate.

From eqs 9 and 10, the segment density profile can be written as

$$\rho_l(\boldsymbol{r}) = \int\sum_{j=1}^{m_l}\delta(\boldsymbol{r} - \boldsymbol{r}')\exp[\beta\mu_{M,l} - \beta U_{M,l} - \beta V_{M,l} - \sum_{i=1}^{m_l}\lambda_l(\boldsymbol{r}_i)]\,\mathrm{d}\boldsymbol{R}_l \tag{11}$$

where

$$\lambda^{(l)}_{hs}(\boldsymbol{r}) = \beta f^{(l)}_{hs}[\bar{\rho}^{(l)}_{hs}(\boldsymbol{r})] + \sum_{i=1}^{L}\sum_{k=1}^{L}\int\rho_i(\boldsymbol{r}')\frac{\delta\beta f^{(i)}_{hs}[\bar{\rho}^{(i)}_{hs}(\boldsymbol{r})]\delta\bar{\rho}^{(k)}_{hs}(\boldsymbol{r}')}{\delta\bar{\rho}^{(k)}_{hs}(\boldsymbol{r}')\quad\delta\rho_l(\boldsymbol{r})}\,\mathrm{d}\boldsymbol{r}' \tag{12a}$$

$$\lambda^{(l)}_{attr}(\boldsymbol{r}) = \beta f^{(l)}_{attr}[\bar{\rho}^{(l)}_{attr}(\boldsymbol{r})] + \sum_{i=1}^{L}\sum_{k=1}^{L}\int\rho_i(\boldsymbol{r}')\frac{\delta\beta f^{(i)}_{attr}[\bar{\rho}^{(i)}_{attr}(\boldsymbol{r})]\delta\bar{\rho}^{(k)}_{attr}(\boldsymbol{r}')}{\delta\bar{\rho}^{(k)}_{attr}(\boldsymbol{r}')\quad\delta\rho_l(\boldsymbol{r})}\,\mathrm{d}\boldsymbol{r}' \tag{12b}$$

Equation 11 can be used to solve the segment density profile; however, we need to know the intramolecular interaction $U_{M,l}$. Following previous studies,[42−45] $U_{M,l}$ can be obtained by a

single-chain Monte Carlo (MC) simulation, and subsequently, the density profiles arecalculated by

$$\rho_l(\boldsymbol{r}) = \exp(\beta\mu_{M,l})\langle\int\sum_{j=1}^{m_l}\delta(\boldsymbol{r}-\boldsymbol{r}')\exp[-\beta U_{M,l}-\sum_{i=1}^{m_l}\lambda_l(\boldsymbol{r}_i)]\,d\boldsymbol{R}_l\rangle \quad (13)$$

where $\langle ... \rangle$ is the ensemble average for a single chain.

In addition to a single-chain MC simulation, we also performed a multi-chain MC simulation to test our theoretical predictions. As used previously by Dickman and Hall,[52] two types of trial moves including translation and chain jiggling were carried out to sample polymer chain(s). For a typical system, about 10^7 trial moves were used for sampling. In translation, a randomly selected chain is translated with a random displacement in the *x*, *y*, or *z* direction. In jiggling, each bond is subject to a random rotation. The polar angle θ and the azimuthal angle ϕ of the new bond are supposed to uniformly distribute between $[0,\theta_{max}]$ and $[0,2\pi]$, respectively. Here, θ_{max} is a maximum angle governed by the acceptance ratio. Specifically, three steps are involved to generate discrete points of $(\theta,\phi) \in [0,\theta_{max}] \times [0,2\pi]$. First, a random number $\kappa \in [\cos\theta_{max},1]$ is generated according to

$$\kappa = \cos\theta_{max} + (1-\cos\theta_{max})\varpi \quad (14)$$

where ϖ is a random number uniformly distributed within (0,1). Second, a random number ξ is generated between 0 and 1, and the two angles (θ,ϕ) are given by

$$\theta = \arccos\kappa \qquad \phi = 2\pi\xi \quad (15)$$

Third, the Cartesian coordinates are calculated by

$$x = \sin\theta\cos\phi \qquad y = \sin\theta\sin\phi \qquad z = \cos\theta \quad (16)$$

By doing these, random variables are obtained that uniformly distribute in a certain angle on a spherical surface.

3. Results and Discussion

In the calculations demonstrated below, two-component equimolar homopolymer mixtures A_{m_a}/B_{m_b} are confined to a slit with width $H = 10\sigma$ in the *z* direction. While m_a is fixed at 3, m_b varies at 3, 6, 9, and 12 to examine the chain length effect of the second component. The square-well depths are given by $\epsilon_{BB}/\epsilon_{AA} = 0.5$ and $\epsilon_{AB} = \sqrt{\epsilon_{AA}\epsilon_{BB}}$, and the reduced temperature is set as $T^* = kT/\epsilon_{AA} = 6.0$. The total packing fraction of the polymer mixture inside the slit is fixed at $\eta = (\pi/6)\sum_l^K m_l\rho_{M,l}\sigma_l^3 = 0.1$.

3.1. Density Profiles. Figure 1 shows the density profiles of the A_3/B_6 mixture in a selective slit with $\lambda_{AW} = -0.5$ and $\lambda_{BW} = 1.0$ predicted from this work and the previous DFT,[31] respectively, along with simulation data. Although in a nonselective slit, the previous DFT was found to match well with simulation,[31] in the selective slit here, it deviates appreciably from simulation. The hybrid DFT of this work shows remarkable agreement with simulation over the entire range $z = 0 \sim 3\sigma$. Compared with the previous DFT, the hybrid DFT accounts for the intramolecular correlation substantially well by integrating single-chain simulation.

Figure 2 shows the density profiles of the A_3/B_{m_b} ($m_b = 6$, 12) mixture in a selective slit with $\lambda_{AW} = -1.0$ and $\lambda_{BW} = 1.0$. B_{m_b} is adsorbed while A_3 is depleted on the selective slit; consequently, segment density of B_{m_b} is always larger than that of A_3 at $z < 1.7\sigma$, and B_{m_b} exhibits a peak or a cusp at $z = \sigma$.

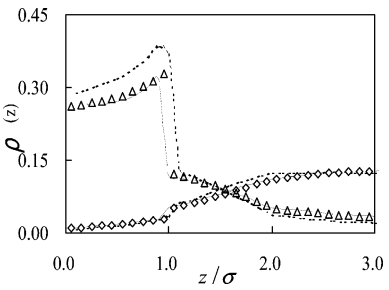

Figure 1. Density profiles of the A_3/B_6 mixture in a selective slit ($\lambda_{AW} = -0.5$ and $\lambda_{BW} = 1.0$). ◇, A_3 and Δ, B_6. Solid lines, this work; dashed lines, Ye et al.'s work;[31] symbols, simulations.

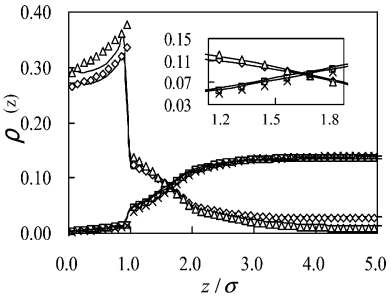

Figure 2. Density profiles of the A_3/B_{m_b} ($m_b = 6$, 12) mixture in a selective slit ($\lambda_{AW} = -1.0$ and $\lambda_{BW} = 1.0$). □, A_3 and ◇, B_6 in the A_3/B_6 mixture; ×, A_3 and Δ, B_{12} in the A_3/B_{12} mixture. Lines, predictions; symbols, simulations.

This behavior of B_{m_b} represented here is similar to pure fluid near a square-well wall.[30,53−55] The preferential adsorption of B_{m_b} is simply due to the selective slit wall that attracts B_{m_b} but repels A_3. In general, our DFT agrees well with simulation, though it slightly underestimates the density within $0 < z < \sigma$. As mentioned, by employing single-chain simulation to take into account intramolecular correction, our hybrid DFT is superior to the previous DFT. Nevertheless, more appropriate weighting functions should be introduced to further improve the accuracy. Beyond $z = \sigma$, the density of B_{m_b} decreases gradually while the density of A_3 increases upon reaching constant. The density profiles also depict that there is a sharp separation between A_3 and B_{m_b}, and apparently, the selectivity depends on the polymer chain length. The larger the difference is between the two components, the greater the separation is.

Figure 3 shows the effect of λ_{BW} on the density profiles of the A_3/B_6 mixture in a selective surface with $\lambda_{AW} = -0.5$. The theoretical predictions are in good accordance with simulation data at various λ_{BW}. With increasing λ_{BW} (i.e., the adsorption energy between segment B and slit becomes stronger), the adsorption of B_6 (Figure 3b) and the depletion of A_3 (Figure 3a) near the slit wall are enhanced. At a very large adsorption energy (e.g., $\lambda_{BW} = 10.0$), B_6 forms double adsorption layers (double cusps) partially due to the excluded-volume effect. In contrast, at a small adsorption energy (e.g., $\lambda_{BW} = 1.0$) there is only one adsorption layer caused by the configurational entropy effect. The discontinuity in the density profiles at $z = \sigma$ (both Figure 3a and Figure 3b) is simply related to the square-well potential.

3.2. Configurations. Figure 4 shows the center-of-mass density profiles of the A_3/B_{m_b} ($m_b = 6$, 12) mixture in a selective slit with $\lambda_{AW} = -1.0$ and $\lambda_{BW} = 1.0$. The density ρ_{center} is normalized by the average density $\rho_{av-center} = (H\sigma)^{-1}\int_0^{H\sigma}\rho_{center}(z)\,dz$. Because the slit attracts chain B_{m_b} and repels chain A_3, there is a depletion for A_3 and adsorption for B_{m_b}.

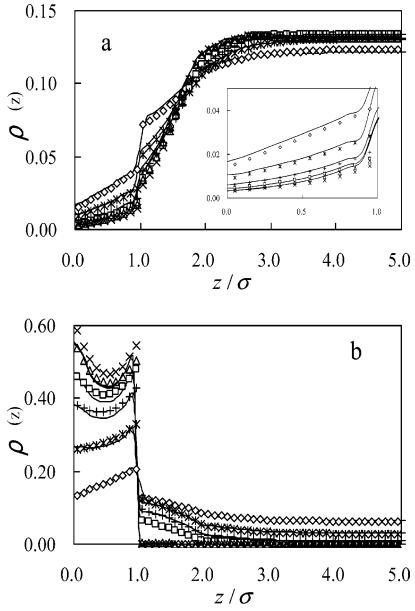

Figure 3. Density profiles of the A_3/B_6 mixture in a selective slit ($\lambda_{AW} = -0.5$ and various λ_{BW}). ◇, $\lambda_{BW} = 0.5$; *, $\lambda_{BW} = 1.0$; +, $\lambda_{BW} = 1.5$; □, $\lambda_{BW} = 2.0$; Δ, $\lambda_{BW} = 5.0$; ×, $\lambda_{BW} = 10.0$. Lines, predictions; symbols, simulations. (a) A_3 and (b) B_6.

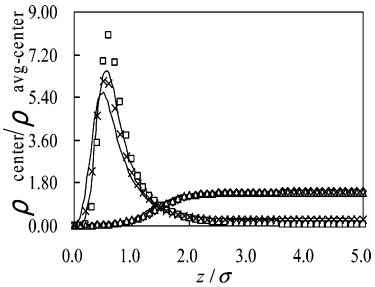

Figure 4. Center-of-mass density profiles of the A_3/B_{m_b} ($m_b = 6$, 12) mixture in a selective slit ($\lambda_{AW} = -1.0$ and $\lambda_{BW} = 1.0$). Δ, A_3 and ×, B_6 in the A_3/B_6 mixture; ◇, A_3 and □, B_{12} in the A_3/B_{12} mixture. Lines, predictions; symbols, simulations.

The extent of depletion or adsorption enhances with increasing adsorption or repulsion energy (data not shown). As m_b becomes larger, the chain connectivity effect in B_{m_b} becomes more important, and thus, the density of B_{m_b} increases. The theoretical predictions for the density profile of B_{m_b} in the mixture are more accurate than those in previous work,[31] as mentioned, because the intramolecular interaction is well accounted for in this work.

Figure 5 shows the radii of gyration of the A_3/B_{m_b} ($m_b = 6$, 12) mixture in a selective slit with $\lambda_{AW} = -1.0$ and $\lambda_{BW} = 1.0$. Our theory captures the essential trends fairly well upon comparison with simulation data. Because the interaction between B_{m_b} and slit is attractive, the adsorbed B_{m_b} molecules are aligned preferentially parallel to the surface, and hence, $\langle(R_{g,xy}/\sigma)^2\rangle$ of B_{m_b} is larger near the surface. Departure from the surface, $\langle(R_{g,xy}/\sigma)^2\rangle$ of B_{m_b} first decreases to a minimum, then increases slightly, and finally approaches a constant. In contrast, $\langle(R_{g,zz}/\sigma)^2\rangle$ of B_{m_b} exhibits the reversed behavior. Because A_3 is depleted, the segment−segment interaction rather than the segment−surface interaction is predominant for $\langle(R_{g,xy}/\sigma)^2\rangle$ of A_3 near the surface.

Adsorption configurations can typically be classified into three types: tail, loop, and train. A sequence of successive segments are referred to as a tail if they start from the head or the end of a chain to the first segment in contact with the surface; the

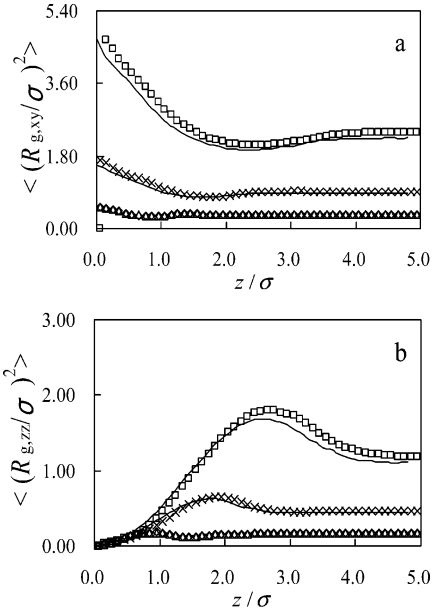

Figure 5. Radii of gyration of the A_3/B_{m_b} ($m_b = 6$, 12) mixture in a selective slit ($\lambda_{AW} = -1.0$ and $\lambda_{BW} = 1.0$). Δ, A_3 and ×, B_6 in the A_3/B_6 mixture; ◇, A_3 and □, B_{12} in the A_3/B_{12} mixture. Lines, predictions; symbols, simulations. (a) $\langle(R_{g,xy}/\sigma)^2\rangle$ and (b) $\langle(R_{g,zz}/\sigma)^2\rangle$.

segments are referred to as a loop if they are between two nearest segments that are in contact with the surface, and they are referred to as a train if there are a sequence of successive segments that are in contact with the surface. Consequently, the lengths of the tail, loop, and train are in the range between 1 and m_{l-1}, m_{l-2}, and m_l, respectively. Additionally, a bridge is also observed for a sufficiently long polymer chain adsorbed simultaneously on both surfaces. This type of configuration is closely related to the stability of colloidal suspensions. By using single-chain simulation, the sizes and percentages of adsorption configurations are calculated for the first time from DFT.

The probability $P_q(i)$ of finding a configuration with i beads is defined as[56−58]

$$P_q(i) = N_q(i)/\sum N_q(i) \tag{17}$$

where q = tail, loop, train, or bridge. $N_q(i)$ is the total number of a configuration q with i beads. The average size of a configuration is given by[56−58]

$$\langle i\rangle_q = \sum_i iP_q(i)/\sum_i P_q(i) \tag{18}$$

The percentage S_q of a configuration is defined as[57]

$$S_q = \sum_i i \times N_q(i)/\sum_q\sum_i i \times N_q(i) \tag{19}$$

Figure 6 shows the average sizes and percentages of tail, loop and train in B_6 of the A_3/B_6 mixture in a selective slit with $\lambda_{AW} = -0.5$ and different λ_{BW}. With increasing adsorption energy between segment B and surface (i.e., increasing λ_{BW}), more B_6 molecules are adsorbed. As a consequence, $\langle i\rangle_{tail}$ in B_6 decreases, while $\langle i\rangle_{loop}$ and $\langle i\rangle_{train}$ increase (Figure 6a); S_{tail} decreases, while S_{loop} increases (Figure 6b). Nevertheless, the extent of decrease or increase is not pronounced. Beyond a certain λ_{BW}, as we shall see in Figure 8a, the adsorption reaches saturation. In this situation, the excluded-volume effect becomes more important, and the average sizes and percentages of the configurations change marginally. Because the surface is repulsive to segment A, A_3 is much less adsorbed than B_6. Furthermore, λ_{BW} has little effect on the configurations in A_3. Upon increasing λ_{BW},

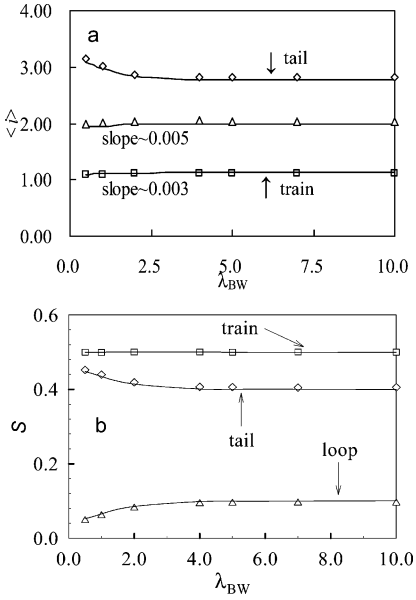

Figure 6. (a) Average sizes and (b) percentages of tail, loop, and train in B_6 of the A_3/B_6 mixture in a selective slit ($\lambda_{AW} = -0.5$ and various λ_{BW}) ◇, tail; Δ, loop; □, train. Lines, predictions; symbols, simulations.

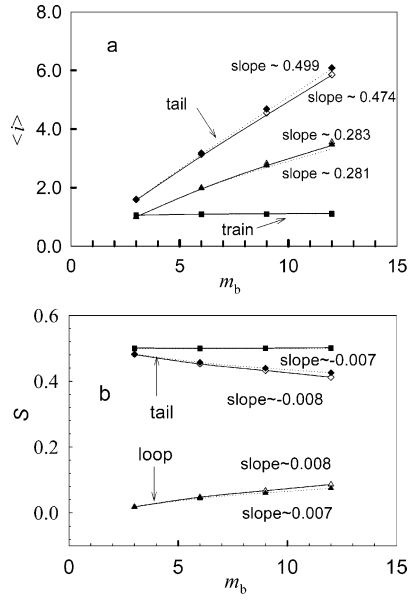

Figure 7. (a) Average sizes and (b) percentages of tail, loop, and train in B_{m_b} of the A_3/B_{m_b} ($m_b = 3, 6, 9, 12$) mixture in a selective slit ($\lambda_{AW} = -0.5$ and $\lambda_{BW} = 0.5$) ◇, tail; Δ, loop; □, train; and in a nonselective slit ($\lambda_{AW} = \lambda_{BW} = 0.5$) ◆, tail; ▲, loop; ■, train. Lines, predictions; symbols, simulations.

$\langle i \rangle_{tail}$, $\langle i \rangle_{loop}$, and $\langle i \rangle_{train}$ in A_3 nearly remain the same, approximately equal to 1.75, 1.00, and 1.03, respectively.

Figures 7 shows the average sizes and percentages of tail, loop, and train in B_{m_b} of the A_3/B_{m_b} ($m_b = 3, 6, 9, 12$) mixture in a selective slit with $\lambda_{AW} = -0.5$ and $\lambda_{BW} = 0.5$ and in a nonselective slit with $\lambda_{AW} = \lambda_{BW} = 0.5$. In the selective slit, with increasing chain length of B_{m_b}, while the relative amount of B_{m_b} in the mixture decreases because as mentioned earlier the total packing fraction is fixed at 0.1, the average sizes and percentages of the three configurations increase except S_{tail}. The lengths of tail, loop, and train are primarily governed by chain length, and a longer chain naturally leads to longer configurations. Though not shown, the average sizes of configurations in A_3 remain almost constant. Similar chain-length dependences of the configurations were previously predicted by the

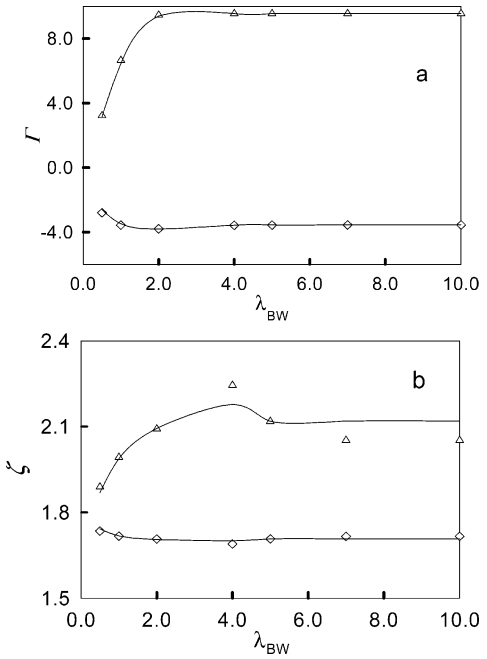

Figure 8. (a) Adsorption amounts and (b) layer thicknesses of the A_3/B_6 mixture in a selective slit ($\lambda_{AW} = -0.5$ and various λ_{BW}). ◇, A_3; Δ, B_6. Lines, predictions; symbols, simulations.

Scheutjens−Fleer lattice theory[59] and observed in a detailed atomistic simulation for polyethylene melt adsorbed on graphite.[60] For still longer B_{m_b} chain, for example, $m_b = 16$, bridges are observed to form connecting the two slit surfaces with a very small percentage $\sim 10^{-6}$. Upon increasing further $m_b = 24$, both size and percentage of bridge are enhanced to 18.5 and 10^{-4}, respectively.

Quite similar configurational behavior is found in the nonselective slit. The average sizes of the three configurations in A_3 are nearly constant, in which $\langle i \rangle_{tail}$ is about 1.60, slightly smaller than that in the selective slit; $\langle i \rangle_{loop}$ and $\langle i \rangle_{train}$ are approximately the same as those in the selective slit. Figures 6 and 7 reveal that nearly half adsorbed polymer chains present are tails, and the other half are trains.

3.3. Adsorption Amounts and Layer Thicknesses. Adsorption amount is defined as

$$\Gamma = \sum_{i=1}^{H\times h} (\rho_i - \rho_b^{(i)}) \tag{20}$$

where ρ_i and $\rho_b^{(i)}$ are the local density in the slit and the bulk density of segment i. Following Scheutjens and Fleer,[59] we define the root-mean-square layer thickness as

$$\zeta^2 = \sum_{i=1}^{H\times h} (i/H)^2 \rho_i / \sum_{i=1}^{H\times h} h\rho_i \tag{21}$$

Once the density profile is known, both adsorption amount and layer thickness can be readily estimated.

Figure 8 shows the adsorption amounts Γ and layer thicknesses ζ of the A_3/B_6 mixture in a selective slit with $\lambda_{AW} = -0.5$ and various λ_{BW}. Note that A_3 is depleted from the slit surface; consequently, its Γ is negative. As λ_{BW} initially increases (i.e., the adsorption energy increases), the adsorption amount increases in B_6 and decreases in A_3. Accordingly, the layer thickness of B_6 increases, and that of A_3 decreases. With further increasing λ_{BW}, Γ approaches a plateau for either A_3 or B_6, but interestingly, ζ exhibits a maximum for B_6 at $\lambda_{BW} =$

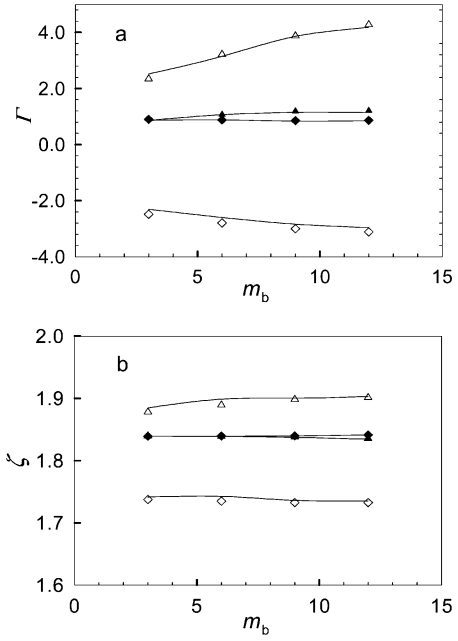

Figure 9. (a) Adsorption amounts (b) and layer thicknesses of the A_3/B_{m_b} ($m_b = 3, 6, 9, 12$) mixture in a selective slit ($\lambda_{AW} = -0.5$ and $\lambda_{BW} = 0.5$) ◇, A_3; Δ, B_{m_b}; and in a nonselective slit ($\lambda_{AW} = \lambda_{BW} = 0.5$) ◆, A_3; ▲, B_{m_b}. Lines, predictions; symbols, simulations.

4.0. At λ_{BW} between 4.0 and 7.0, ζ decreases by a small extent. This is because the initially formed adsorption layer is relatively loose and tends to be compact upon further adsorption. Finally, at $\lambda_{BW} > 7.0$, the excluded-volume effect is dominant, and consequently, ζ reaches a constant.

Figure 9 shows the adsorption amounts Γ and layer thicknesses ζ of the A_3/B_{m_b} ($m_b = 3, 6, 9, 12$) mixture in a selective slit with $\lambda_{AW} = -0.5$ and $\lambda_{BW} = 0.5$ and in a nonselective slit with $\lambda_{AW} = \lambda_{BW} = 0.5$. In the selective slit, with an increase of m_b, both the adsorption amount Γ and the layer thickness ζ in B_{m_b} increase because of the effect of chain connectivity; however, they decrease in A_3. In the nonselective slit, A_3 and B_{m_b} exhibit nearly the same adsorption amount and layer thickness.

3.4. Partition Coefficients. The adsorption of each component in mixture can be characterized by the partition coefficient defined as

$$K_i = \rho_{av}^{(i)}/\rho_b^{(i)} \tag{22}$$

where $\rho_{av}^{(i)}$ and $\rho_b^{(i)}$ are the average density in the slit and the bulk density of segment *i*. The selectivity between the two polymers in mixture is quantified by the relative partition coefficient of the component *i* over *j*

$$K_r = K_i/K_j \tag{23}$$

Figure 10 shows the partition coefficients of the A_3/B_6 mixture in a selective slit with $\lambda_{AW} = -0.5$ and various λ_{BW}. With increasing adsorption energy between segment B and slit wall (i.e., λ_{BW} increases), K_A changes negligibly while K_B increases significantly. At a low λ_{BW} (e.g., 1.0), K_B depends on the competition between the configurational entropy and the segment−wall interaction. At a high λ_{BW} (e.g., 4.0), λ_{BW} plays a predominant role and K_B tends to be infinity. The relative partition $K_r = K_A/K_B$ decreases with increasing λ_{BW}. At a low λ_{BW}, the segment−segment interaction is dominant, and the selectivity between A_3 and B_6 is not distinct. At a high λ_{BW},

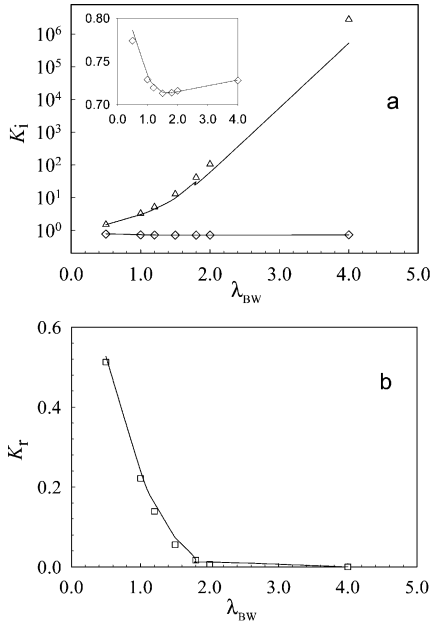

Figure 10. Partition coefficients of the A_3/B_6 mixture in a selective slit ($\lambda_{AW} = -0.5$ and various λ_{BW}). ◇, K_A; Δ, K_B; □, K_r. Lines, predictions; symbols, simulations.

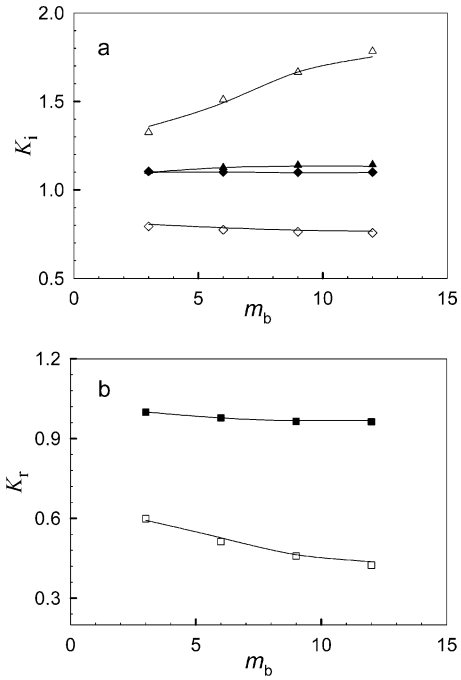

Figure 11. Partition coefficients of the A_3/B_{m_b} ($m_b = 3, 6, 9, 12$) mixture in a selective slit ($\lambda_{AW} = -0.5$ and $\lambda_{BW} = 0.5$) ◇, K_A; Δ, K_B; □, K_r; and in a nonselective slit ($\lambda_{AW} = \lambda_{BW} = 0.5$) ◆, K_A; ▲, K_B; ■, K_r. Lines, predictions; symbols, simulations.

the segment−wall interaction and the excluded-volume effect dominate the segment−segment interaction and lead to a greater selectivity. Beyond $\lambda_{BW} = 1.8$, K_r is nearly equal to zero. This indicates that there are only B_6 exists in the slit and A_3 is almost completely excluded.

Figure 11 shows the partition coefficients of the A_3/B_{m_b} ($m_b = 3, 6, 9, 12$) mixture in a selective slit with $\lambda_{AW} = -0.5$ and $\lambda_{BW} = 0.5$ and in a nonselective slit with $\lambda_{AW} = \lambda_{BW} = 0.5$. In the selective slit, K_B increases, and K_A decreases upon increasing the chain length of m_b. This is a result of the chain connectivity, and the effect appears more notable with further increasing m_b. While B_{m_b} is adsorbed more, A_3 is depleted away from the slit

because of the excluded-volume effect. With a larger m_b, K_r departs further away from unity. This suggests that the separation between A_3 and B_{m_b} is enhanced. In the nonselective slit, K_A and K_B are about the same and depend very weakly on m_b. As a result, K_r is approximately equal to unity implying no separation between the two polymers.

4. Conclusions

We have developed a hybrid DFT to study the structural and thermodynamic features of homopolymer mixtures confined in a nanoslit. Theoretical predictions are presented for two-component mixtures under a wide range of conditions. The theory shows excellent agreement with simulation data for the density profiles, adsorption configurations, adsorption amounts, layer thicknesses, and partition coefficients. Because of the hybridized single-chain simulation, our DFT is accurate even at very strong segment−wall affinity and is superior to previous DFTs.

The results reveal that both the segment−wall interaction and the polymer chain length have pronounced effects on the confined behavior. In a selective slit, one polymer is preferentially adsorbed while the other is depleted. The radii of gyration is governed by the segment−wall interaction for adsorbed polymer and by the segment−segment interaction for nonadsorbed polymer. When the length of the longer polymer chain in the mixture increases, the chain connectivity effects become more important. There is a critical adsorption energy at which the adsorption layer thickness exhibits a maximum. While the density profiles and separation factors are largely influenced by the segment−wall interaction, the effect on the adsorption configurations is relatively small. Adsorbed molecules are present predominantly as tails and trains. In addition, bridges are observed to form for sufficiently long polymer chains.

Acknowledgment. The authors are grateful to the referees for helpful comments. This work was supported by the National Natural Science Foundation of China (Project Nos. 20676030 and 20490200), the Doctoral Research Foundation sponsored by the Ministry of Education of China (Project No. 20050251004), E-institute of Shanghai High Institution Grid (No. 200303), the Shanghai Municipal Education Commission of China, and the National University of Singapore.

References and Notes

(1) Sheldon, R. A. *J. Chem. Technol. Biotechnol.* **1996**, *67*, 1.
(2) Maier, G. *Angew. Chem., Int. Ed.* **1998**, *37*, 2960.
(3) Koros, W. J.; Mahajan, R. *J. Membr. Sci.* **2000**, *175*, 181.
(4) Buchholz, B. A.; Doherty, E. A. S.; Albarghouthi, M. N.; Bogdan, F. M.; Zahn, Z. M.; Barron, A. E. *Anal. Chem.* **2001**, *73*, 157.
(5) Madabhushi, R. S. *Electrophoresis* **1998**, *19*, 224.
(6) Liao, X.; Lu, Z.; Shi, B. *Ind. Eng. Chem. Res.* **2003**, *42*, 3397.
(7) Lu, Y.; Bennick, A. *Arch. Oral Biol.* **1998**, *43*, 717.
(8) Wang, D.; Chen, B.; Ji, J.; Feng, L. *Bioconjugate Chem.* **2002**, *13*, 792.
(9) Kilduff, J. E.; Wigton, A. *Environ. Sci. Technol.* **1999**, *33*, 250.
(10) Qi, N.; LeVan, M. D. *Ind. Eng. Chem. Res.* **2005**, *44*, 3726.
(11) Heuchel, M.; Snurr, R. Q.; Buss, E. *Langmuir* **1997**, *13*, 6795.
(12) Dunne, J. A.; Rao, M.; Sircar, S.; Gorte, R. J.; Myers, A. L. *Langmuir* **1997**, *13*, 4333.
(13) Linse, P.; Hatton, T. A. *Langmuir* **1997**, *13*, 4066.
(14) Bai, R.; Yang, R. T. *Langmuir* **2005**, *21*, 8326.
(15) Egorov, A. *J. Phys. Chem. B* **2001**, *105*, 6583.
(16) Szabelski, P.; Nieszporek, K. *J. Chem. Phys.* **2003**, *107*, 12296.
(17) Duda, Y.; Pizio, O.; Sokolowski, S. *J. Chem. Phys.* **2004**, *108*, 19442.
(18) Pigorini, G.; LeVan, M. D. *Ind. End. Chem. Res.* **1997**, *36*, 2306.
(19) Pigorini, G.; LeVan, M. D. *Ind. End. Chem. Res.* **1999**, *38*, 2439.
(20) Ladanyi, B. M.; Chandler, D. *J. Chem. Phys.* **1975**, *62*, 4308.
(21) Chandler, D.; McCoy, J. D.; Singer, S. J. *J. Chem. Phys.* **1986**, *85*, 5971.
(22) Chandler, D.; McCoy, J. D.; Singer, S. J. *J. Chem. Phys.* **1986**, *85*, 5977.
(23) McCoy, J. D.; Singer, S. J.; Chandler, D. *J. Chem. Phys.* **1987**, *87*, 4853.
(24) Hooper, J. B.; Pileggi, M. T.; McCoy, J. D.; Gurro, J. G.; Weinhold, J. D. *J. Chem. Phys.* **2000**, *112*, 3094.
(25) Woodward, C. E. *J. Chem. Phys.* **1991**, *94*, 3183.
(26) Kierlik, E.; Rosinberg, M. L. *J. Chem. Phys.* **1994**, *100*, 1716.
(27) Nath, S. K.; Nealey, P. F. *J. Chem. Phys.* **1999**, *110*, 7483.
(28) Cai, J.; Liu, H.; Hu, Y. *Fluid Phase Equilib.* **2002**, *281*, 194−197.
(29) Zhang, S.; Cai, J.; Liu, H.; Hu, Y. *Mol. Simul.* **2004**, *30*, 143.
(30) Ye, Z.; Cai, J.; Liu, H.; Hu, Y. *J. Chem. Phys.* **2005**, *123*, 194902.
(31) Ye, Z.; Chen, H.; Cai, J.; Liu, H.; Hu, Y. *J. Chem. Phys.* **2006**, *125*, 124705.
(32) Ye, Z.; Chen, H.; Liu, H.; Hu, Y.; Jiang, J. *J. Chem. Phys.*, accepted.
(33) Yu, Y.-X.; Wu, J. *J. Chem. Phys.* **2002**, *117*, 2368.
(34) Rosenfeld, Y. *Phys. Rev. Lett.* **1989**, *63*, 980.
(35) Zhou, S. Q.; Zhang, X. Q. *Phys. Rev. E* **2001**, *64*, 011112.
(36) Tripathi, S.; Chapman, W. G. *J. Chem. Phys.* **2005**, *122*, 094506.
(37) Chapman, W. G.; Jackson, G.; Gubbins, K. E. *Mol. Phys.* **1988**, *65*, 1057.
(38) Bryk, P.; Bucior, K.; Sokolowski, S.; Zukocinski, G. *J. Phys. Chem. B* **2005**, *109*, 2977.
(39) Yu, Y.; Wu, J.; You, F.; Gao, G. *Chin. Phys. Lett.* **2005**, *22*, 246.
(40) Goel, T.; Patra, C. N.; Ghosh, S. K.; Mukherjee, T. *J. Chem. Phys.* **2004**, *121*, 4865.
(41) Yu, Y. X.; Gao, G. H.; Wang, X. L. *J. Phys. Chem. B* **2006**, *110*, 14418.
(42) Yethiraj, A.; Woodward, C. E. *J. Chem. Phys.* **1995**, *102*, 5499.
(43) Cao, D.; Jiang, T.; Wu, J. *J. Chem. Phys.* **2006**, *124*, 164904.
(44) Cao, D.; Wu, J. *J. Chem. Phys.* **2004**, *121*, 4210.
(45) Cao, D.; Zhu, M.; Wang, W. *J. Phys. Chem. B* **2006**, *110*, 21882.
(46) Yethiraj, A.; Fynewever, H.; Shew, C.-Y. *J. Chem. Phys.* **2001**, *114*, 4323.
(47) Sen, S.; Cohen, J. M.; McCoy, J. D.; Curro, J. G. *J. Chem. Phys.* **1994**, *101*, 9010.
(48) Yu, Y.-X.; Wu, J. *J. Chem. Phys.* **2003**, *118*, 3835.
(49) Patra, C. N.; Yethiraj, A. *J. Chem. Phys.* **2000**, *112*, 1579.
(50) Hu, Y.; Liu, H.; Prausnitz, J. M. *J. Chem. Phys.* **1996**, *104*, 396.
(51) Gil-Villegas, A.; Galindo, A. *J. Chem. Phys.* **1997**, *106*, 4168.
(52) Dickman, R.; Hall, C. K. *J. Chem. Phys.* **1988**, *89*, 3168.
(53) Zhou, S. *J. Phys. Chem. B* **2003**, *107*, 3585.
(54) Henderson, J. R.; van Swol, F. *J. Chem. Phys.* **1988**, *89*, 5010.
(55) Cao, D.; Wu, J. *Macromolecules* **2005**, *38*, 971.
(56) Jeon, J.; Dobrynin, A. V. *Phys. Rev. E: Stat. Phys., Plasmas, Fluids, Relat. Interdiscip. Top.* **2003**, *67*, 061803.
(57) Chen, H.; Ye, Z.; Peng, C.; Liu, H.; Hu, Y. *J. Chem. Phys.* **2006**, *125*, 204708.
(58) Chen, H.; Peng, C.; Ye, Z.; Liu, H.; Hu, Y.; Jiang, J. *Langmuir* **2007**, *23*, 2430.
(59) Scheutjens, J. M. H. M.; Fleer, G. J. *Macromolecules* **1985**, *18*, 1882.
(60) Daoulas, K. C.; Harmandaris, V. A.; Mavrantzas, V. G. *Macromolecules* **2005**, *38*, 5780.